Published in final edited form as:
Anal Chem. 2008 February 1; 80(3): 665–674. doi:10.1021/ac701807v.

UPLC-ESI-TOFMS-Based Metabolomics and Gene Expression Dynamics Inspector Self-Organizing Metabolomic Maps as Tools for Understanding the Cellular Response to Ionizing Radiation

Andrew D. Patterson[†], **Henghong Li**[‡], **Gabriel S. Eichler**[§], **Kristopher W. Krausz**[†], **John N. Weinstein**[§], **Albert J. Fornace Jr.**[‡], **Frank J. Gonzalez**[†], and **Jeffrey R. Idle**[*,¶]
Laboratory of Metabolism, Center for Cancer Research, National Cancer Institute, National Institutes of Health, Bethesda, Maryland, Lombardi Comprehensive Cancer Research Center, Georgetown University, Washington, District of Columbia, Genomics and Bioinformatics Group, Laboratory of Molecular Pharmacology, Center for Cancer Research, National Cancer Institute, National Institutes of Health, Bethesda, Maryland, and Institute of Clinical Pharmacology, University of Bern, Switzerland

Abstract

Global transcriptomic and proteomic profiling platforms have yielded important insights into the complex response to ionizing radiation (IR). Nonetheless, little is known about the ways in which small cellular metabolite concentrations change in response to IR. Here, a metabolomics approach using ultraperformance liquid chromatography coupled with electrospray time-of-flight mass spectrometry was used to profile, over time, the hydrophilic metabolome of TK6 cells exposed to IR doses ranging from 0.5 to 8.0 Gy. Multivariate data analysis of the positive ions revealed dose- and time-dependent clustering of the irradiated cells and identified certain constituents of the water-soluble metabolome as being significantly depleted as early as 1 h after IR. Tandem mass spectrometry was used to confirm metabolite identity. Many of the depleted metabolites are associated with oxidative stress and DNA repair pathways. Included are reduced glutathione, adenosine monophosphate, nicotinamide adenine dinucleotide, and spermine. Similar measurements were performed with a transformed fibroblast cell line, BJ, and it was found that a subset of the identified TK6 metabolites were effective in IR dose discrimination. The GEDI (Gene Expression Dynamics Inspector) algorithm, which is based on self-organizing maps, was used to visualize dynamic global changes in the TK6 metabolome that resulted from IR. It revealed dose-dependent clustering of ions sharing the same trends in concentration change across radiation doses. “Radiation metabolomics,” the application of metabolomic analysis to the field of radiobiology, promises to increase our understanding of cellular responses to stressors such as radiation.

High-throughput studies of the molecular and cellular effects of ionizing radiation (IR) have depended on “omic”1 profiling technologies, particularly genomic, transcriptomic, and proteomic platforms.2–6 Such efforts have discovered IR-induced perturbations of DNA, RNA, and protein molecules and have been successful in developing markers that provide information about IR-induced phenomena such as the threshold dose.4,7,8 Furthermore, integrating data from combinations of such platforms, in the spirit of emerging systems biology, has given investigators the ability to reconstruct and analyze IR-responsive

* Corresponding author. Phone: +420 603 484 583. Fax: +420 220 912 140. E-mail: jeff.idle@ikp.unibe.ch.
[†]Laboratory of Metabolism, Center for Cancer Research.
[‡]Georgetown University.
[§]Laboratory of Molecular Pharmacology, Center for Cancer Research.
[¶]University of Bern.

pathways.9 However, pathways generated from such analyses remain incomplete without similar global measurements of metabolite concentrations. Despite recent advances in metabolic profiling technologies, changes in small-molecule concentration remain underexplored and underexploited. That is particularly unfortunate because, as the end-products of transcriptional and/or proteomic signaling events, metabolites may represent the most incisive and accurate indicators of the state of cellular physiology.10

Metabolomics is a rapidly advancing field that aims to characterize the concentration changes of all small molecules existing in a biofluid.11 Application of metabolomic technologies to the understanding of physiology, toxicology, and disease progression has led to appreciable advances by defining novel drug and carcinogen metabolites,12–15 as well as biomarkers of disease.16,17 At the same time, the metabolomic technologies have contributed to a general understanding of how metabolites and their concentrations change under defined conditions.18 However, in contrast to transcriptomics and proteomics, broad-based metabolomic studies have not been used to analyze the cellular effects of IR. Small-scale, directed approaches using high-sensitivity nuclear magnetic resonance spectroscopy (NMR)19–23 have been applied to estimate the relative concentration changes of a small subset of metabolites (e.g., reduced glutathione) following IR, but a global metabolomic approach has not yet been reported. The effects of IR include activation of stress responses to reduce reactive oxygen species (ROS), an increase in nucleotide pools for unscheduled DNA repair, and increases in cellular energy intermediates. All of those effects call for concerted metabolomic investigation. Also, given the growing body of evidence suggesting that IR-responsive targets, such as the tumor suppressor p53, can have profound effects on metabolic pathways,24,25 a comprehensive overview of the “radiation metabolome” would give investigators another vantage point from which to understand the effects of IR exposure.

For assessment of the potential application of metabolomics to radiobiology, a UPLC-ESI-TOFMS metabolomic assay was established to evaluate the changes in small-molecule concentration that occur after γ-irradiation of cells in culture. The high-resolution of ultraperformance liquid chromatography (UPLC) and the accurate mass measurement of electrospray ionization time-of-flight mass spectrometry (ESI-TOFMS) were combined to generate protonated molecular ion matrices consisting of peak areas identified by specific m/z values and retention times. The hydrophilic metabolomes of the lymphoid TK6 cell line and the hTERT-transformed fibroblast BJ cell line were analyzed following different doses of IR over a period of 16 h. The overall aim was to evaluate the utility of metabolomics as a tool for interrogating the cellular physiology and pharmacology of cultured cells and, specifically, to generate a clearer understanding of the metabolite concentration changes that take place after IR. Standard multivariate statistical analyses were complemented by the first application in metabolomics of the GEDI (Gene Expression Dynamics Inspector) algorithm, which used self-organizing maps to generate a global visualization of the responses to IR.

EXPERIMENTAL SECTION

Chemicals

Adenosine monophosphate, debrisoquine hemisulfate, glutathione (reduced), nicotinamide, 5-oxoproline, proline, calcium phosphorylcholine chloride, guanosine 5′-monophosphate, uridine 5′-monophosphate, β-nicotinamide adenine dinucleotide, and spermine were purchased from Sigma-Aldrich (St. Louis, MO). All other reagents and solvents were HPLC grade.

Cell Culture

TK6 cells (a lymphoblastic cell line derived from a patient with hereditary spherocytosis) were cultured in RPMI 1640 growth medium supplemented with 10% heat-inactivated fetal bovine serum (Invitrogen, Carlsbad, CA) and maintained in a humidified 37 °C incubator with 5% CO_2. hTERT-transformed BJ cells were cultured in Knockout DMEM (Invitrogen) supplemented with 199 medium (Invitrogen), 15% fetal bovine serum, Pen/Strep, and L-glutamine. From a stock flask of exponentially growing cells, 2×10^5 TK6 cells/mL were seeded into T75 flasks and cultured for 16 h before exposure to 0.5, 1.0, 4.0, or 8.0 Gy γ-radiation from a ^{137}Cs source. BJ cells were seeded into 100 cm^2 plates and cultured for 48 h before exposure to 1.0 and 4.0 Gy γ-irradiation. Control cells were sham-irradiated by placing them in the irradiator without exposure to the ^{137}Cs source. Dose rates were as follows: 0.5 Gy = 0.37 Gy/min, 1.0 Gy = 0.85 Gy/min, 4.0 Gy = 1.76 Gy/min, and 8.0 Gy = 2.84 Gy/min. After irradiation, TK6 cells were divided into six T25 flasks for each dose. The irradiated TK6 cells were returned to the incubator for 1, 4, 8, or 16 h, at which point they were spun down, washed twice with ice-cold PBS, and frozen as pellets at −70 °C. For the BJ cells, after irradiation they were returned to the incubator for 1, 4, or 16 h, at which point they were washed twice with ice-cold PBS, scraped, and frozen as pellets at −70 °C.

Sample Preparation

Cell pellets were resuspended in 150 μL of water and briefly sonicated to liberate the water-soluble fraction of metabolites. A 20 μL aliquot was removed to determine total protein concentration by the BCA assay (Pierce, Madison, WI). Each cell extract was mixed with an equal volume of 50% acetonitrile acid containing 1 μM debrisoquine hemisulfate as internal standard and spun at 16 000*g* for 20 min at 4 °C. The supernatant was dried down in an evaporating centrifuge and resuspended in 300 μL of HPLC grade water. Last, the supernatant was passed over an Ultrafree-MC column (Millipore Corporation, Bedford, MA) to remove particulates larger than 0.2 μm. The eluent was frozen at −70 °C until analysis.

Western Blotting

TK6 cells were harvested 2 h following IR and analyzed by Western blotting to assess cellular levels of phospho-p53 at serine residue 15 and phosphohistone γH2AX at serine residue 139 (Cell Signaling Technology, Beverly, MA). Total extracellular signal-related kinase (ERK, p42) was used for the loading control (Cell Signaling Technology).

UPLC-ESI-TOFMS Analysis

An aliquot of each cell pellet supernatant was deposited in an autosampler vial, and 5 μL was separated on a 50 mm × 2.1 mm Acquity 1.7 μm C18 column (Waters Corp, Milford, MA) using an Acquity UPLC system (Waters). The gradient mobile phase consisted of 0.1% formic acid (A) and acetonitrile containing 0.1% formic acid (B). A typical 10 min sample run consisted of 0.5 min of 100% solvent A followed by an incremental increase of solvent B up to 100% for the remaining 9.5 min. The flow rate was set to 0.6 mL/min. The eluent was introduced by electrospray ionization into the mass spectrometer (Waters QTOF Premier) operating in positive ionization mode. The capillary and sampling cone voltages were set to 3000 and 30 V, respectively. Source and desolvation temperatures were set to 120 and 350 °C, respectively, and the cone and desolvation gas flows were set to 50.0 and 650.0 L/h, respectively. To maintain mass accuracy, sulfadimethoxine ($[M + H]^+$ = 311.0814) at a concentration of 500 pg/μL in 50% acetonitrile was used as a lock mass and injected at a rate of 0.08 μL/min. For MS scanning, data were acquired in centroid mode from 50 to 850 m/z, and for MS/MS, the collision energy was ramped from 5 to 35 V.

Multivariate Data Analysis (MDA)

The mass chromatographic data were first analyzed by MarkerLynx (Waters) to generate a multivariate data matrix for analysis by SIMCA-P+ 11 software (Umetrics, Kinnelon, NJ). The matrices were purged of known instrument artifacts, normalized by the debrisoquine internal standard peak area, and trimmed to contain only the 1000 most abundant molecular ions. Principal components analysis (PCA) and partial least-squares discriminant analysis (PLS-DA) were performed on Pareto-scaled26 MarkerLynx matrices to identify candidate metabolites that could distinguish irradiated cells from the shams. For that purpose, loadings scatter plots were used to identify ion peak areas whose intensities significantly differed between sham and irradiated samples. Models were validated for fit (R^2) and predictability (Q^2) by randomly permuting the samples 200 times and recalculating R^2 and Q^2. Models were considered acceptable if R^2 and Q^2 degraded with permutation of the samples.

Molecular Ion Identification

Metabolites identified as being altered in intensity between sham and irradiated cells were subjected to further scrutiny to determine their elemental compositions. MassLynx software and Seven Golden Rules27 were used to determine putative elemental compositions, and metabolites were verified using tandem MS by comparison with authentic compounds.

Protonated Molecular Ion Quantitation

Peak areas obtained from the MarkerLynx matrices were used to calculate relative concentrations by first normalizing all samples by the peak area from the debrisoquine internal standard ($C_{10}H_{14}N_3^+$ = 176.1188) and then dividing by the total protein concentration. Finally, relative concentrations were determined by dividing the peak areas from each irradiated sample by that from the respective sham-irradiated control.

Statistical Analysis and GEDI Self-Organizing Maps

The significance of the relative concentration for each metabolite was assessed by ANOVA with Bonferroni correction. Gene Expression Dynamics Inspector (GEDI)28 was used for analysis and visualization of patterns in the MarkerLynx data matrices. The software package was developed for, and applied in the past to, the interpretation of gene expression data. This is its first use in metabolomics. GEDI creates intuitive visualizations of each sample based on the self-organizing map (SOM) algorithm. However, it improves the interpretability of typical SOMs by rendering the output for each experimental sample as a two-dimensional heat-map-like mosaic of colored tiles. GEDI starts by training a conventional SOM to assign each ion to a mosaic tile in such a way that ions with similar patterns across the samples are placed in the same or nearby tiles. After that training, GEDI, unlike the conventional SOM algorithm, creates a series of coherent mosaic heat maps representing each sample's overall ion profile. The GEDI analysis here used Pearson's correlation as the similarity metric in training of the SOM. In addition, to identify the common expression patterns within each dose group, GEDI was used to compute average mosaics. The complete GEDI program package and details of the algorithm can be found at http://www.childrenshospital.org/research/ingber/GEDI/gedihome.htm.

RESULTS AND DISCUSSION

Monitoring IR Dose by Traditional Techniques

TK6 cells are widely used as a model system to study the effects of IR at the cellular level. For demonstration that TK6 cells used in the metabolomic studies had been dosed as indicated and that they displayed dose-dependent responses, the phosphorylation of p53-(Ser15) and γH2AX(Ser139) was monitored 2 h after IR exposure by Western blot. These

two phosphorylations are representative protein level indicators of IR response. As seen in Figure 1, dose-dependent increases in phosphorylation were observed consistent with published results for both p53(Ser15)29 and γH2AX(Ser139).30

Multivariate Data Analysis of Irradiated Cells Demonstrates Dose-Dependent Effects on the Metabolome

Cell extracts containing hydrophilic metabolites from the irradiated TK6 cells were analyzed by UPLC-ESI-TOFMS operating in positive ionization mode. The resulting MS peak areas were then profiled using MDA to identify metabolites whose concentrations were significantly altered by IR. With the use of SIMCA-P+, principal components analyses (not shown), and supervised PLSDA two-component models were generated from the MarkerLynx data matrices. At 1 h after IR, there was already class separation between the sham and the four IR doses (Figure 2A). The most pronounced differences were those among three prominent clusters consisting of sham-irradiated cells, 0.5 and 1.0 Gyirradiated cells, and 4.0 and 8.0 Gy-irradiated cells. To provide an internal validation measure, the data were randomized 200 times and, after each randomization, R^2 (a measure of model fit) and Q^2 (a measure of model predictive capacity) values were recalculated. The data were then plotted to indicate metabolomic responses, using the sham-irradiated samples as baseline (not shown). Validation analysis for the 0.5, 1.0, and 4.0 Gy doses suggested that the model fit was modest, but the predictive function, as measured by Q^2, remained acceptable for those doses. The 8.0 Gy dose model fit was acceptable, as both R^2 and Q^2 values degraded with permutation of the data. Similar observations were recorded for the 4, 8, and 16 h time points; 16 h, class separation, particularly at doses below 4.0 Gy, was less apparent (Figure 2B–D). One of the 16 h samples irradiated with 8.0 Gy was considered an outlier as it fell beyond the confidence limits defined by the Hotelling ellipse and was excluded from all further analyses (Figure 2D). The protein concentration of this sample was found to be significantly lower compared to other samples suggesting inefficient isolation and extraction of metabolites. Overall, from the first hour after irradiation a clear dose-related perturbation of the cell metabolome was observed over the entire range from 0.5 to 8.0 Gy.

A similar UPLC-ESI-TOFMS approach as described above was used to profile cell extracts containing hydrophilic metabolites from a BJ fibroblast cell line. This cell line was chosen for its normal diploid karyotype. As observed with the TK6 cells, the two-component PLS-DA models successfully discriminated the sham-, 1.0 Gy-, and 4.0 Gy-irradiated cells over 16 h (Figure 3A–C). One sham-irradiated sample (low protein concentration) was excluded from this and all other analyses as it fell beyond the confidence limits defined by the Hotelling ellipse. Inclusion of BJ cell metabolomics data demonstrated the general applicability of UPLC-ESI-TOFMS and MDA toward understanding the effects of IR on the metabolome.

Identification of Biochemical Constituents of the TK6 Cell Metabolome Down-Regulated by γ-Irradiation

Loadings plots from the TK6 cells were analyzed to identify ions with the highest confidence (i.e., those with the smallest confidence intervals) and greatest contribution to separation. The most significant ions contributing to class separation 1 h after irradiation were those down-regulated after IR (Figure 4, upper-right quadrant). Protonated molecular ions 308.0908 and 348.0694 ranked as the first and second most important variables from the loadings plots, respectively (Table 1). Chemical formula calculations on those ions showed that they correspond to reduced glutathione (GSH) and adenosine monophosphate (AMP), respectively. Among the other highest-contributing ions were in-source fragment ions of GSH (ions 5, 11, and 13, plus the Na^+ adduct, ion 20) and AMP (ion 3). Other biochemical constituents of the TK6 cellular metabolome that were attenuated by irradiation

included nicotinamide and nicotinamide adenine dinucleotide (NAD^+), proline and 5-oxoproline, phosphocholine, uridine monophosphate (UMP), and spermine. Thus, UPLC-ESI-TOFMS afforded ready chromatographic resolution of the cellular metabolome and determination of accurate masses that permitted preliminary assignment of the constituents (with m/z errors ranging from 0.9 to 9.8 ppm; mean 3.8). Comparison of the MS/MS fragmentation patterns obtained from authentic compounds and from the cell supernatants then unequivocally verified the identities of those protonated molecular ions and also confirmed the identity of any in-source fragment ions (Figure 5). Molecular ions whose identities remained unknown were not evaluated further.

It should be stated that, despite the power of UPLC-ESITOFMS in analyzing a complex biological matrix, it is not without limitations. Of particular note is the relative inability of the UPLC system to retain and resolve very small highly polar metabolites, for example, isomers, such as citrate and isocitrate. In circumstances where resolution of such isomeric metabolites was required, it would be necessary to utilize a platform such as GCTOF with chemical derivatization of cell extracts.

Identification of Biochemical Constituents of the TK6 Cell Metabolome Up-Regulated by γ-Irradiation

The lower-left quadrant of Figure 4 displays ions that are more abundant in irradiated than in sham-irradiated cells at 1 h. None of those ions made a statistically significant contribution to the class separation at the 1 h time point, so they were not investigated further. However, other subsets of the metabolome (e.g., the lipidome) may have potential as biomarkers that increase in response to IR. Additionally, other detection methods (e.g., gas chromatography) may be useful in identifying other metabolites not readily observed by UPLC-ESI-TOFMS.

Dose-Dependent IR-Induced Changes in the Metabolome

Although much is known about the effects of IR at the transcriptomic and proteomic levels, much less information is available about IR effects on the metabolome, particularly at biologically relevant doses (less than 10 Gy). For assessment of possible metabolomic changes at those doses, UPLC-ESI-TOFMS analyses were performed to quantitate the dose-dependent changes in specific metabolite concentration as well as to validate the significance of those ions found to be important in the MDA loadings plot. Protonated molecular ion intensities were normalized to the internal standard debrisoquine and then to total protein in order to assess whether a dose-dependent relationship existed with any identified metabolites. At 1 h following IR, subtle but statistically significant decreases in some of the metabolome constituents, including AMP, glutathione, NAD^+, and spermine, were observed (Figure 6). At 4 h after IR, the effects observed at 1 h had been partially lost, and at 8 h after IR, no significant differences between sham and irradiated metabolomes could be detected. However, at 16 h after IR, the decreases in concentration of glutathione, NAD^+, and spermine at doses of 4.0 and 8.0 Gy remained significantly different from those in the sham-irradiated cells. Particularly at 16 h after IR, changes in these metabolites may be early signs of cell death as lymphoid cells such as TK6 readily undergo apoptosis after 24 h with doses as low as 1.0 Gy.[31]

Analysis of the BJ metabolome constituents similarly revealed GSH, NAD^+, and spermine to be important indicators of IR exposure (AMP levels fell below the limit of detection for this cell line and were not recorded in the chromatographic data). At 1 h following 1.0 Gy, a significant increase was observed in GSH concentration (Figure 7). However, like the TK6 cells, both GSH and NAD^+ concentrations were depleted at 4 h after 4.0 Gy. Unlike the TK6 cells at 16 h after IR, BJ cell NAD^+ and spermine concentrations remained unchanged for all doses at this time point, while GSH concentration was elevated with 4.0 Gy of IR. These

observations may reflect the cell type specific IR-induced programmatic response. Importantly, along with the TK6 data, those observations highlight the potential importance of GSH and NAD^+ in the IR metabolomic response.

Visualization of the Global Metabolomic Response to Irradiation

Significant bottlenecks in any LC/MS-based metabolomic investigation are the lack of metabolome annotation and the paucity of methods for visualization of the metabolomic data set as a whole. Because of those limitations, the SOM algorithm in the GEDI software package was used to construct visualizations reflecting the relationships among positive ions on the basis of abundance patterns across the entire TK6 data set. When presented in that fashion, the hydrophilic metabolome could be viewed in its entirety by clustering related metabolites in the same or closely neighboring tiles (Figure 8A). The 16 h postirradiation data were used since, at the level of individual molecular ions, a trend suggestive of a dose–response relationship was apparent at that time point. Protonated molecular ions derived from GSH (308.0908), AMP (348.0694), and spermine (203.2227) clustered in the same general location on the map (Figure 8A, lower black rectangle), despite being ions ranked number 1, 2, and 70 in their contribution to group separation between irradiated and sham-irradiated cells. That is so because they covaried across the entire set of samples, and, therefore, GEDI's SOM algorithm placed them in closely neighboring tiles. A clear dose-dependent effect on specific subsets of the hydrophilic metabolome was apparent, as represented graphically for the down-regulated (Figure 8B) and up-regulated (Figure 8C) pools of 188 and 219 metabolites, respectively.

Published studies support the view that cellular metabolites are altered after irradiation of cells. Those previous studies focused on concentration changes of specific metabolites20 or, in some cases, defined metabolic effects at high doses of radiation (20–40 Gy).20,21,23 Those limitations precluded identification of the metabolites most significantly affected or biologically relevant to an in vivo or in vitro IR response. However, with the advent of high-throughput, high-sensitivity technologies that permit global and unbiased analysis of the metabolome, such determinations are now possible. Particularly when coupled with contemporary data analysis approaches such as MDA and SOMs, those approaches can become powerful tools for both studying and visualizing the metabolome response to IR at doses less than 10 Gy. As shown in Figures 2 and 3, discrete clustering of cell samples after exposure to lower doses (0.5 and 1.0 Gy) and higher doses (4.0 and 8.0 Gy) was apparent in the TK6 and BJ cell data sets analyzed here.

The biological relevance of metabolites such as glutathione,32 spermine,33–36 and their precursors is well documented in the radiation literature. Glutathione, a tripeptide (L-γ-glutamyl-L-cysteinylglycine), is highly abundant in the cell and is a major antioxidant. It protects the cell from the deleterious effects of ROS during normal metabolic processes (e.g., respiration) or following exposure to IR. Furthermore, the glutathione concentration in the cell is strongly associated with cellular radioresistance (i.e., the higher the glutathione concentration, the more radioresistant the cell), and many therapies, such as buthionine sulfoximine, that target the synthesis of glutathione, are useful for increasing the cell-killing effect of IR.23 The differences observed between TK6 and BJ cells with GSH likely reflect a cell-specific response to IR and may be due to differences existing between normal and transformed phenotype of cells. Spermine is a polyamine that associates primarily with the DNA helix and protects against DNA damage through chromatin compaction.35 In TK6 cells, the decline in cellular 5-oxoproline, a metabolite and a precursor of glutathione, may also be related to the quenching of cellular glutathione by γ-radiation. Therefore, it is not surprising to find that glutathione and spermine were identified as major contributors in the MDA analysis of irradiated cells (Figures 2 and 3).

In TK6 cells, the reasons for the decrease in AMP concentration after IR are less apparent. Possibilities include the generation of ATP to supply the cell with energy to repair IR-induced damage (2ADP = ATP + AMP by adenylate kinase), assistance in the repair of DNA double-strand breaks,37 antioxidant activity (adenosine is a known radical scavenger38), or anabolic function as a dATP precursor. Interestingly, when supplied with exogenous adenosine in the form of AMP, hematogenous cells are protected by reduction of the deleterious effects of IR.37–42 Similarly, the quenching of cellular GMP (as indicated from the guanine fragment ion) and UMP, both nucleic acid building blocks, may simply reflect increased DNA repair and synthesis 1 h postirradiation.

For both cell types, the fall in cellular NAD^+ concentration at 4 h may simply indicate the use of NAD^+ by poly(ADP–ribose)-polymerase, which is activated in response to DNA double- or single-strand breaks.43 Indeed, it has been reported that NAD^+ levels fall 5-fold in Chinese hamster ovary cells irradiated with 56 Gy.43 At least for TK6 cells, the cellular depletion of nicotinamide, a metabolite of NAD^+, presumably reflects the fall in NAD^+. The decrease in free phosphocholine is a probable indicator of membrane damage (i.e., lipid peroxidation), which is typical of IR.44

In summary, this report shows that the soluble fraction derived from TK6 and BJ cells that were subjected to γ-irradiation from 0.5 to 8.0 Gy can be analyzed successfully by UPLC-ESI-TOFMS and MDA. PLS-DA analysis revealed dose- and time-dependent clustering and identified a set of ions that had been attenuated by irradiation. Among the constituents depleted were antioxidants and related molecules (GSH and 5-oxoproline) as well as probable markers of DNA synthesis and repair (AMP, nicotinamide, guanine, UMP, NAD^+, and spermine). Interestingly, those two sets of metabolites were organized into the same general location in the GEDI display, which provided a global view of changes in the metabolome and demonstrated dose–response relationships for the set of 188 down-regulated cellular metabolites. In the present study, the higher, but still physiologically pertinent, IR doses also up-regulated 219 as yet unidentified cellular metabolites. Future analysis and identification of those metabolites will undoubtedly prove instructive. Overall, the combination of UPLCESI-TOFMS, MDA, and GEDI SOMs offers great promise for the study of metabolic stress responses to IR (and also to drugs, toxic molecules, and physiological factors) at both the cellular and whole-body levels.

Acknowledgments

This work was funded by the National Cancer Institute, Intramural Research Program, Center for Cancer Research, and by NIH (NIAID) Grant U19AI067773-02. A.D.P. was supported by a Pharmacology Research Associate in Training Fellowship from the National Institute of General Medical Sciences. J.R.I. is grateful to U.S. Smokeless Tobacco Company for a Grant for collaborative research.

References

1. Weinstein JN. Science. 1998; 282:628–629. [PubMed: 9841413]
2. Amundson SA, Fornace AJ Jr. Health Phys. 2003; 85:36–42. [PubMed: 12852469]
3. Kis E, Szatmari T, Keszei M, Farkas R, Esik O, Lumniczky K, Falus A, Safrany G. Int J Radiat Oncol, Biol, Phys. 2006; 66:1506–1514. [PubMed: 17069989]
4. Menard C, Johann D, Lowenthal M, Muanza T, Sproull M, Ross S, Gulley J, Petricoin E, Coleman CN, Whiteley G, Liotta L, Camphausen K. Cancer Res. 2006; 66:1844–1850. [PubMed: 16452246]
5. Sreekumar A, Nyati MK, Varambally S, Barrette TR, Ghosh D, Lawrence TS, Chinnaiyan AM. Cancer Res. 2001; 61:7585–7593. [PubMed: 11606398]
6. Szkanderova S, Vavrova J, Hernychova L, Neubauerova V, Lenco J, Stulik J. Radiat Res. 2005; 163:307–315. [PubMed: 15733044]

7. Amundson SA, Do KT, Shahab S, Bittner M, Meltzer P, Trent J, Fornace AJ Jr. Radiat Res. 2000; 154:342–346. [PubMed: 11012342]
8. Amundson SA, Lee RA, Koch-Paiz CA, Bittner ML, Meltzer P, Trent JM, Fornace AJ Jr. Mol Cancer Res. 2003; 1:445–452. [PubMed: 12692264]
9. Whitehead K, Kish A, Pan M, Kaur A, Reiss DJ, King N, Hohmann L, DiRuggiero J, Baliga NS. Mol Syst Biol. 2006; 2:47. [PubMed: 16969339]
10. Fiehn O. Plant Mol Biol. 2002; 48:155–171. [PubMed: 11860207]
11. Griffin JL, Nicholls AW. Pharmacogenomics. 2006; 7:1095–1107. [PubMed: 17054419]
12. Chen C, Ma X, Malfatti MA, Krausz KW, Kimura S, Felton JS, Idle JR, Gonzalez FJ. Chem Res Toxicol. 2007; 20:531–542. [PubMed: 17279779]
13. Chen C, Meng L, Ma X, Krausz KW, Pommier Y, Idle JR, Gonzalez FJ. J Pharmacol Exp Ther. 2006; 318:1330–1342. [PubMed: 16775196]
14. Giri S, Idle JR, Chen C, Zabriskie TM, Krausz KW, Gonzalez FJ. Chem Res Toxicol. 2006; 19:818–827. [PubMed: 16780361]
15. Giri S, Krausz KW, Idle JR, Gonzalez FJ. Biochem Pharmacol. 2007; 73:561–573. [PubMed: 17123469]
16. Kind T, Tolstikov V, Fiehn O, Weiss RH. Anal Biochem. 2007; 363:185–195. [PubMed: 17316536]
17. Salek RM, Maguire ML, Bentley E, Rubtsov DV, Hough T, Cheeseman M, Nunez D, Sweatman BC, Haselden JN, Cox RD, Connor SC, Griffin JL. Physiol Genomics. 2007; 29:99–108. [PubMed: 17190852]
18. Zhen Y, Krausz KW, Chen C, Idle JR, Gonzalez FJ. Mol Endocrinol. 2007; 21:2136–2151. [PubMed: 17550978]
19. Luciani AM, Rosi A, Grande S, Guidoni L, Viti V, Cherubini R, Conzato M. Radiat Prot Dosim. 2002; 99:307–310.
20. Santini MT, Romano R, Rainaldi G, Ferrante A, Indovina P, Motta A, Indovina PL. Anticancer Res. 2006; 26:267–281. [PubMed: 16475707]
21. Grande S, Giovannini C, Guidoni L, Luciani AM, Palma A, Rosi A, Sapora O, Viti V. Radiat Prot Dosim. 2006; 122:205–206.
22. Grande S, Luciani AM, Rosi A, Cherubini R, Conzato M, Guidoni L, Viti V. Int J Cancer. 2001; 96(Suppl):27–42. [PubMed: 11992384]
23. Rosi A, Grande S, Luciani AM, Palma A, Giovannini C, Guidoni L, Sapora O, Viti V. Radiat Res. 2007; 167:268–282. [PubMed: 17316070]
24. Bensaad K, Tsuruta A, Selak MA, Vidal MN, Nakano K, Bartrons R, Gottlieb E, Vousden KH. Cell. 2006; 126:107–120. [PubMed: 16839880]
25. Matoba S, Kang JG, Patino WD, Wragg A, Boehm M, Gavrilova O, Hurley PJ, Bunz F, Hwang PM. Science. 2006; 312:1650–1653. [PubMed: 16728594]
26. van den Berg RA, Hoefsloot HC, Westerhuis JA, Smilde AK, van der Werf MJ. BMC Genomics. 2006; 7:142. [PubMed: 16762068]
27. Kind T, Fiehn O. BMC Bioinf. 2007; 8:105.
28. Eichler GS, Huang S, Ingber DE. Bioinformatics. 2003; 19:2321–2322. [PubMed: 14630665]
29. Saito S, Yamaguchi H, Higashimoto Y, Chao C, Xu Y, Fornace AJ Jr, Appella E, Anderson CW. J Biol Chem. 2003; 278:37536–37544. [PubMed: 12860987]
30. Mahrhofer H, Burger S, Oppitz U, Flentje M, Djuzenova CS. Int J Radiat Oncol, Biol, Phys. 2006; 64:573–580. [PubMed: 16414372]
31. Shi YQ, Wuergler FE, Blattmann H, Crompton NE. Radiat Environ Biophys. 2001; 40:301–308. [PubMed: 11820739]
32. Bump EA, Brown JM. Pharmacol Ther. 1990; 47:117–136. [PubMed: 2195553]
33. Douki T, Bretonniere Y, Cadet J. Radiat Res. 2000; 153:29–35. [PubMed: 10630975]
34. Porciani S, Lanini A, Balzi M, Faraoni P, Becciolini A. Phys Med. 2001; 17(Suppl 1):187–188. [PubMed: 11776256]

35. Warters RL, Newton GL, Olive PL, Fahey RC. Radiat Res. 1999; 151:354–362. [PubMed: 10073674]
36. Becciolini A, Porciani S, Lanini A, Balzi M. Int J Radiat Biol Relat Stud Phys, Chem Med. 1987; 52:767–774. [PubMed: 3316080]
37. Bohacek J, Hosek B, Pospisil M. Life Sci. 1993; 53:1317–1324. [PubMed: 8412492]
38. von Frijtag Drabbe Künzel JK, van der Zee J, Ijzerman AP. Drug Dev Res. 1996; 37:48–54.
39. Hofer M, Mazur L, Pospisil M, Weiterova L, Znojil V. Radiat Res. 2000; 154:217–221. [PubMed: 10931695]
40. Hosek B, Bohacek J, Sikulova J, Pospisil M, Vacek A. Radiat Environ Biophys. 1992; 31:289–297. [PubMed: 1438679]
41. Pospisil M, Hofer M, Netikova J, Pipalova I, Vacek A, Bartonickova A, Volenec K. Radiat Res. 1993; 134:323–330. [PubMed: 8316625]
42. Pospisil M, Hofer M, Netikova J, Viklicka S, Pipalova I, Bartonickova A. Experientia. 1992; 48:253–257. [PubMed: 1547855]
43. Kupper JH, Muller M, Wolf I. Biochem Biophys Res Commun. 1999; 265:525–529. [PubMed: 10558902]
44. Edimecheva IP, Kisel MA, Shadyro OI, Vlasov AP, Yurkova IL. Int J Radiat Biol. 1997; 71:555–560. [PubMed: 9191900]
45. Towsend K, Trevino V, Falciani F, Stewart PM, Hewison M, Campbell MJ. Oncology. 2006; 71:111–123. [PubMed: 17377416]

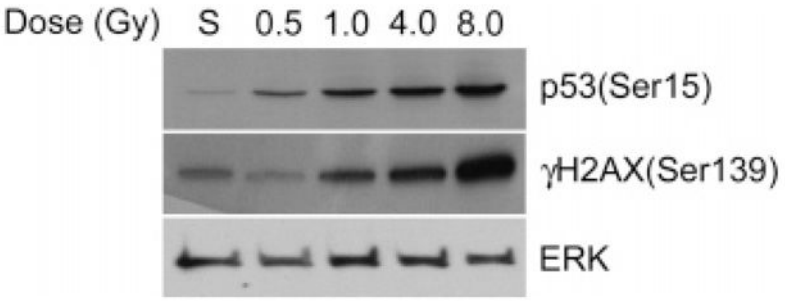

Figure 1.

Western blots showing a dose-dependent increase in phosphorylation of γH2AX(Ser139) and p53(Ser15) after γ-irradiation of TK6 cells. Exponentially growing TK6 cells were irradiated with 0.5, 1.0, 4.0, or 8.0 Gy, and total protein was harvested 2 h later to assess the effects on p53(Ser15) and γH2AX(Ser139). A Western blot of ERK (p42) is included as a loading control.

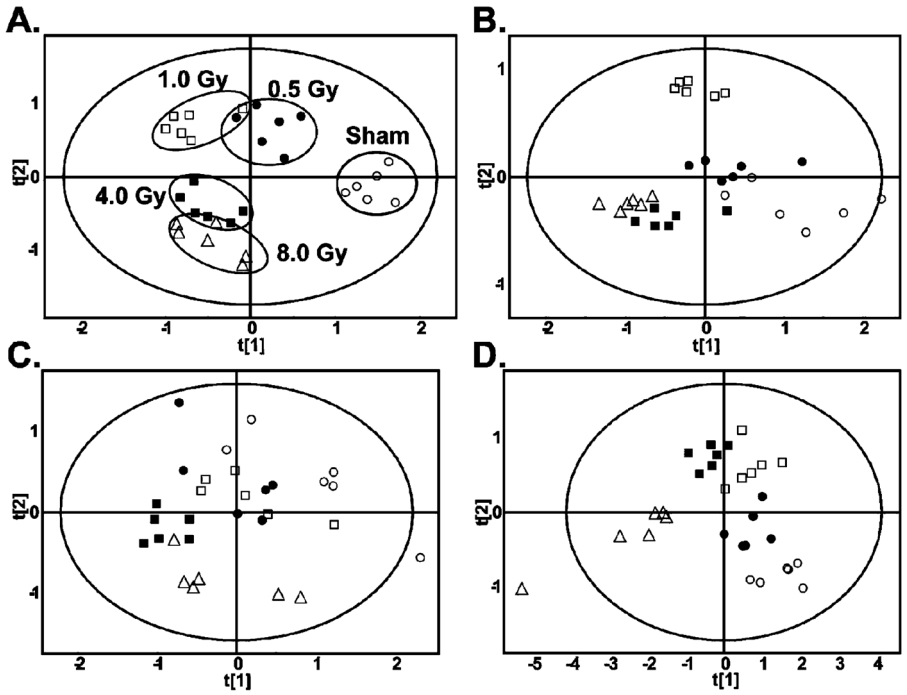

Figure 2.

PLS-DA scores plots demonstrating dose-dependent clustering of irradiated TK6 cells. TK6 cell supernatants were prepared 1 h (A), 4 h (B), 8 h (C), and 16 h (D) after γ-irradiation with 0.5, 1.0, 4.0, or 8.0 Gy and with sham irradiation. One 8.0 Gy-irradiated sample from the 16 h time point (D) located to the extreme left in the scores plot was excluded from all further analyses as it fell beyond the confidence limits defined by the Hotelling ellipse. [t1] and [t2] correspond to principal components 1 and 2, respectively.

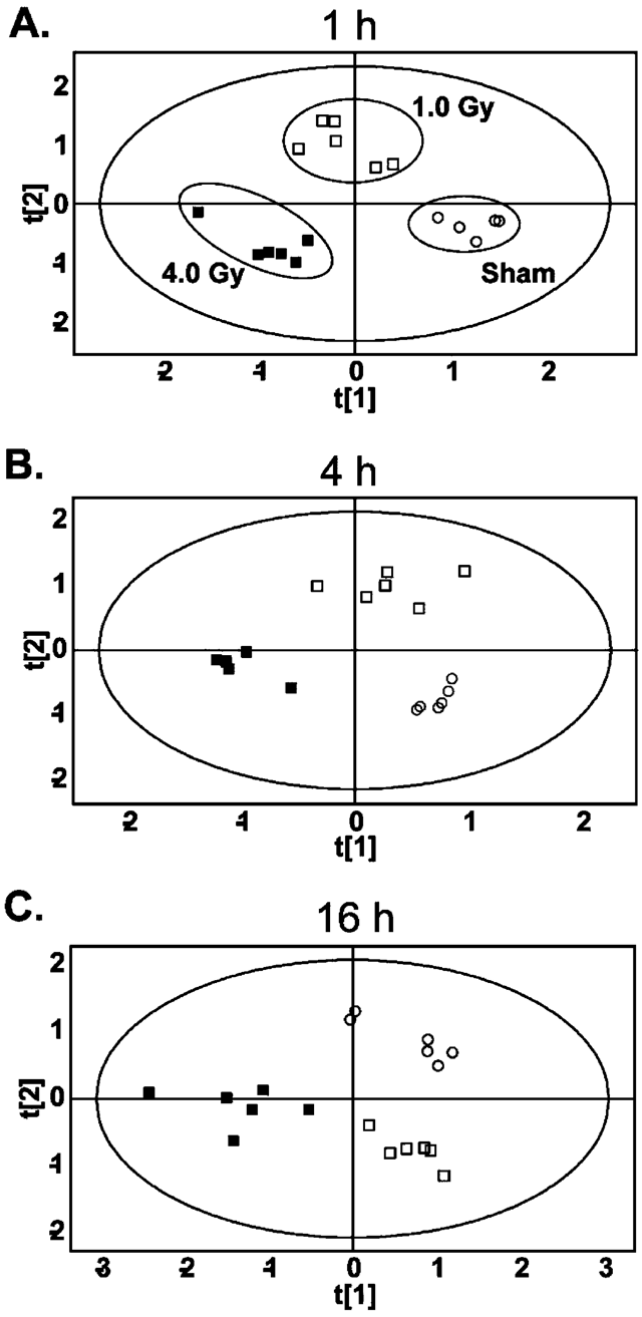

Figure 3.

PLS-DA scores plots demonstrating dose-dependent clustering of irradiated BJ cells. BJ cell supernatants were prepared 1 h (A), 4 h (B), and 16 h (C) after γ-irradiation with 1.0 or 4.0 Gy and with sham irradiation. One sham-irradiated sample at 1 h (A) was excluded from this and all other analyses as it fell beyond the confidence limits defined by the ellipse. [t1] and [t2] correspond to principal components 1 and 2, respectively.

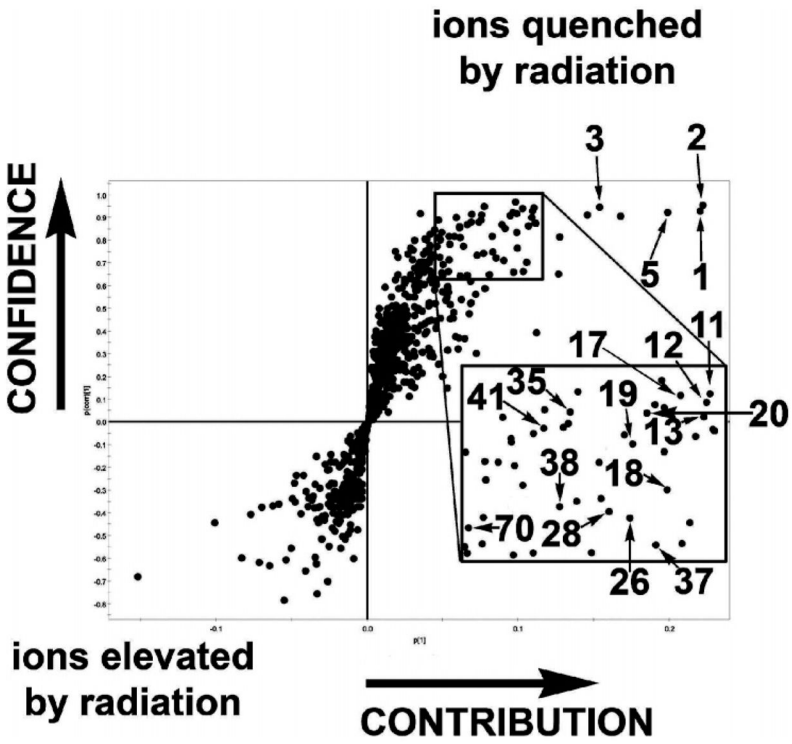

Figure 4.

PLS-DA loadings S-plot comparing supernatants from sham vs 1.0 Gy-irradiated TK6 cells at 1 h after IR showing molecular ions important in the clustering of samples. Positive ions located in the upper right quadrant are quenched when comparing 1.0 Gy- and sham-irradiated cell supernatants. Labeling of ions is the same as in Table 1: 1, GSH; 2, AMP; 3, AMP in-source fragment; 5, GSH in-source fragment; 11, GSH in-source fragment; 12, nicotinamide; 13, GSH in-source fragment; 17, 5-oxoproline; 18, guanine; 19, NAD^+ in-source fragment; 20, GSH Na^+ adduct; 26, phosphocholine; 35, UMP Na^+ adduct; 37, proline; 38, NAD^+; 41, NAD^+ in-source fragment; 70, spermine.

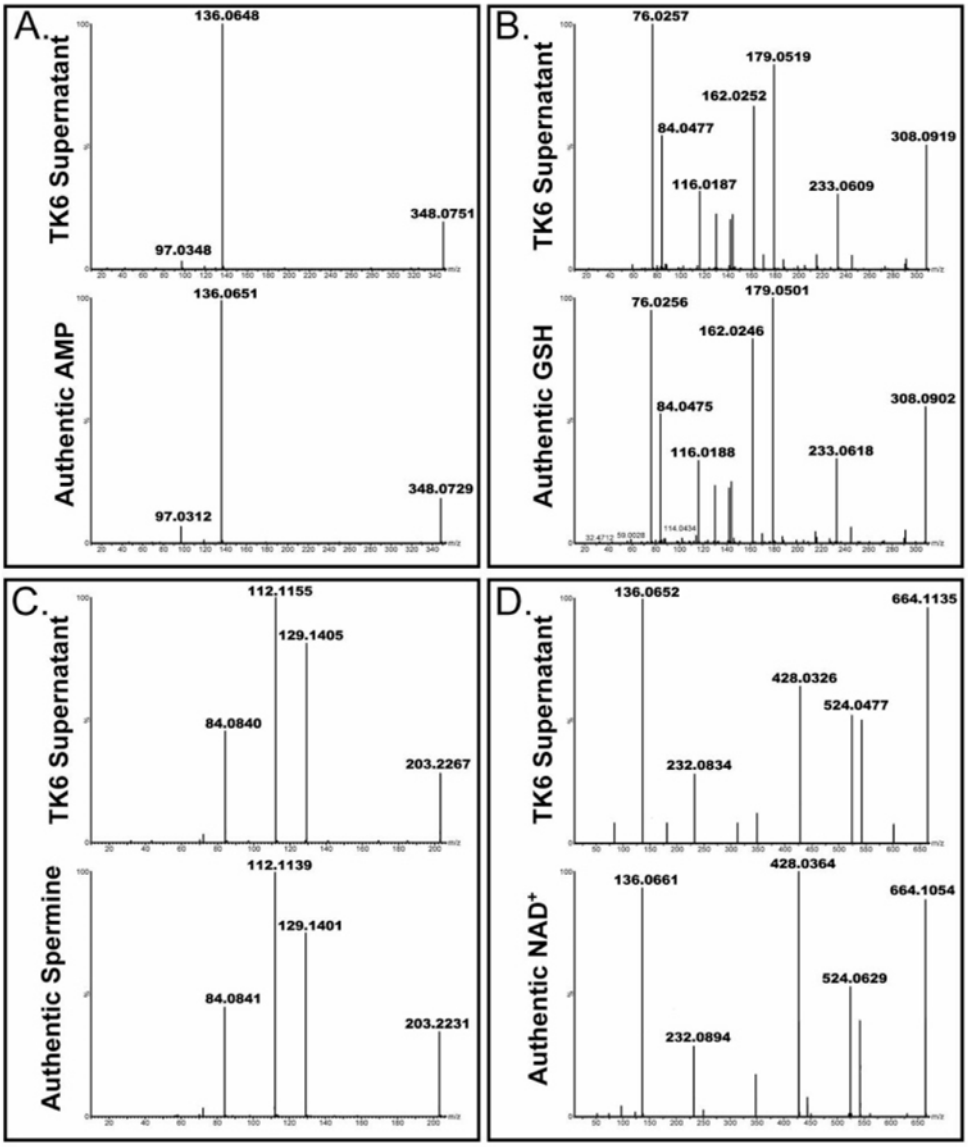

Figure 5.
Tandem MS of molecular ions from cell supernatants and authentic compounds. (A) adenosine monophosphate (AMP), (B) glutathione (GSH), (C) spermine, and (D) nicotinamide adenine dinucleotide (NAD^+).

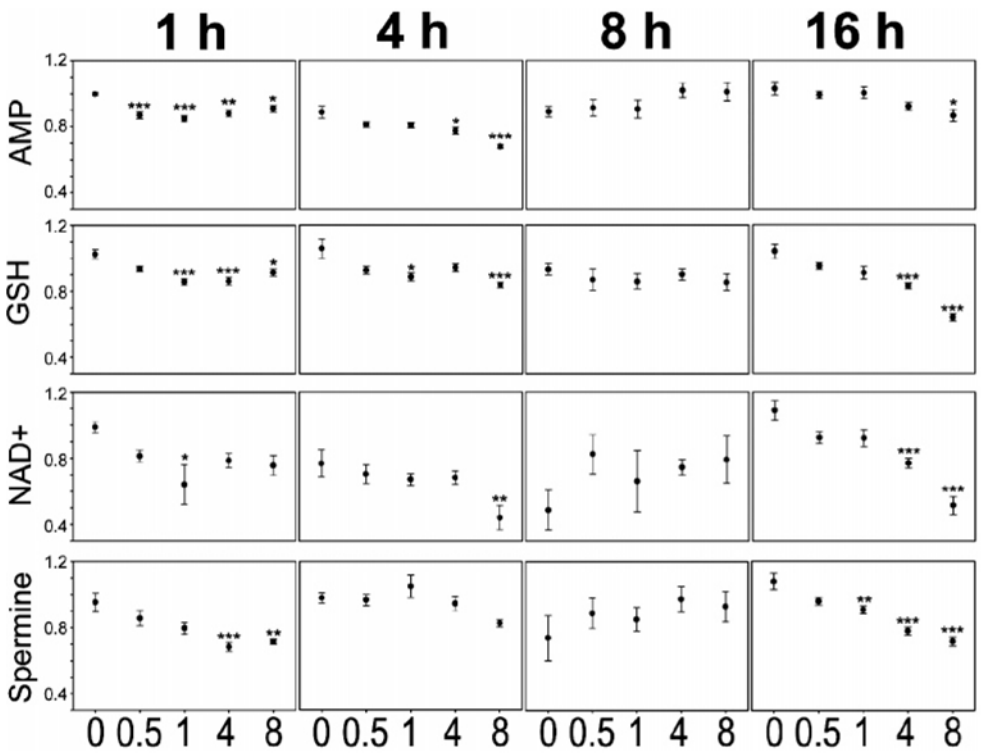

Figure 6.

TK6 cell selected protonated molecular ion peak areas 1, 4, 8, and 16 h after γ-irradiation. Data are plotted as the average of six replicates (16 h 8.0 Gy, $n = 5$) per dose. Error bars represent SEM. The p-values were calculated by ANOVA with Bonferroni correction. * $p < 0.05$, ** $p < 0.01$, *** $p < 0.001$.

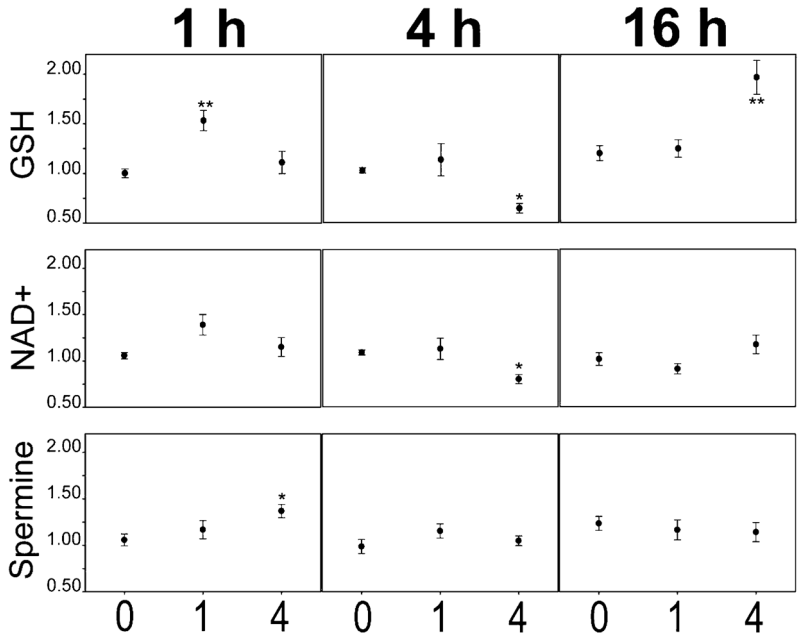

Figure 7.

BJ cell selected protonated molecular ion peak areas 1, 4, and 16 h after γ-irradiation. Data are plotted as the average of six replicates (1 h sham, $n = 5$) per dose. Error bars represent SEM. The p-values were calculated by ANOVA with Bonferroni correction. * $p < 0.05$, ** $p < 0.01$.

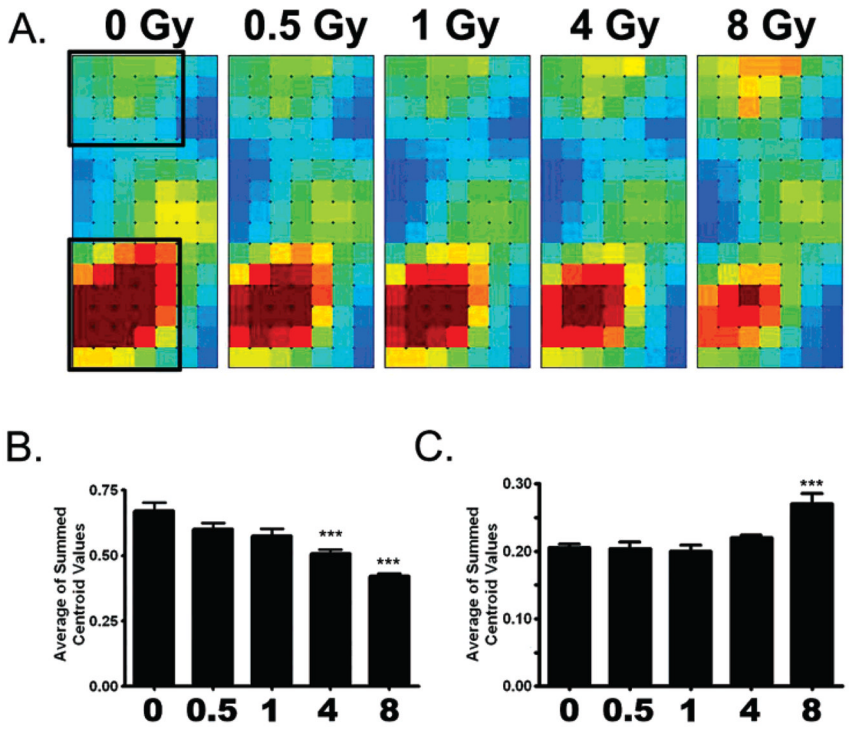

Figure 8.

GEDI analysis using self-organizing maps (SOMs) revealing a dose-dependent effect on the TK6 water-soluble metabolome. (A) SOMs were constructed from MarkerLynx data matrices using Pearson's correlation as the similarity metric, and the average of all replicates (sham (0), 0.5, 1.0, 4.0 Gy, $n = 6$; 8.0 Gy, $n = 5$) was calculated for each dose. Tiles containing the highest-abundance ions are shaded deep red, and the tiles containing the lowest-abundance ions are shaded deep blue. Colors between those extremes reflect a scale of colors typically used in heat maps of gene expression (ref 45). The centroid values were summed for each replicate, averaged, and plotted for (B) the down-regulated metabolite 5 × 6 grid consisting of 188 positive ions (lower black rectangle in panel A) and (C) the up-regulated metabolite 5 × 4 grid consisting of 219 positive ions (upper black rectangle in panel A). Error bars represent SEM. The *p*-values were calculated by ANOVA with Bonferroni correction. *** $p < 0.001$.

Table 1

Characterization of Ions That Are Depleted in the TK6 Cellular Metabolome after 1.0 Gy γ-Irradiation

ion rank	*m/z* (ESI+)	retention time	empirical formula	mass error (ppm)	identity
1	308.0908	0.47	$C_{10}H_{17}N_3O_6S$	2.6	glutathione (reduced, GSH)
2	348.0694	0.40	$C_{10}H_{14}N_5O_7P$	4.3	adenosine monophosphate (AMP)
3	136.0623	0.40			AMP in-source fragment ion
5	179.0495	0.48			GSH in-source fragment ion
11	233.0598	0.47			GSH in-source fragment ion
12	123.0521	0.65	$C_6H_6N_2O$	9.8	nicotinamide
13	162.0229	0.47			GSH in-source fragment ion
17	130.0516	0.30	$C_5H_7NO_3$	9.2	5-oxoproline
18	152.0574	0.48	$C_5H_5N_5O$	1.3	guanosine monophosphate (GMP) in-source fragment
19	136.0705	0.65			NAD^+ in-source fragment ion
20	330.0738	0.47			GSH Na^+ adduct
26	184.0733	0.29	$C_5H_{15}NO_4P$	3.3	phosphocholine
35	347.0263	0.39	$C_9H_{13}N_2O_9P$	2.0	uridine monophosphate (UMP) Na^+ adduct
37	116.0711	0.31	$C_5H_9NO_2$	0.9	proline
38	664.1139	0.64	$C_{21}H_{27}N_7O_{14}P_2$	4.7	nicotinamide adenine dinucleotide (NAD^+)
41	428.0376	0.64	$C_{10}H_{15}N_5O_{10}P_2$	0.9	NAD^+ in-source fragment ion
70	203.2227	0.23	$C_{10}H_{26}N_4$	4.4	spermine